Moment formation in quantum point contacts due to spin-orbit interaction

Jen-Hao Hsiao and Tzay-Ming Hong
Department of Physics, National Tsing Hua University, Hsinchu 300, Taiwan, Republic of China
(Received 26 June 2010; published 14 September 2010)

We demonstrate that a local moment can automatically form in the vicinity of the quantum point contact if we (1) include the spin-orbit interaction and (2) allow the electric field along the longitudinal direction to be both nonuniform and asymmetric. The former breaks the spin degeneracy by introducing an effective magnetic field while the latter ensures that the moment is formed near the point contact where the nonuniformity is the largest. The asymmetry induced by the source-drain bias leads to an imbalance of spin-up and spin-down electrons on different sides of the point contact, which introduces a spin polarization. The nonequilibrium Green's-function formalism is employed to study the transport properties and local spin density. The electron-electron interaction is found to enhance the magnitude of the localized moment, necessary for the Kondo-type scenario of the 0.7 anomaly.

DOI: 10.1103/PhysRevB.82.115309 PACS number(s): 72.25.Dc, 72.10.Bg, 71.10.Fd, 71.70.Ej

I. INTRODUCTION

The quantized conductance ($G_0=2e^2/h$) is one of the characteristics of noninteracting ballistic transport systems. It was predicted by the Landauer formula and first observed in 1988 by the group in Delft[1] with a quantum point contact (QPC) design; namely, a two-dimensional electron gas (2DEG) separated by a pair of side gates. The factor of 2 in the quantized conductance comes from the spin degeneracy. However, an unexpected shoulder often showed up near $0.7G_0$ which has attracted lots of attentions in recent decade.[2] In spite of many theoretical and experimental efforts, the origin of this anomaly remains unsettled.

The spontaneous spin polarization and the Kondo-type effect are separately proposed in two front competing models. The former takes the hint from the smooth evolution of the 0.7 anomaly to $0.5G_0$ upon the application of a magnetic field.[3] It relates the origin of 0.7 anomaly to the *static* spin polarization which was supported by an elegant experiment[4] by Rokhinson *et al.* via the magnetic focusing technique. However, Frolov *et al.*[5] failed to observe the polarization in a nonlocal measurement geometry which they specially designed to enhance the sensitivity to spin transport. We suppose this discrepancy is probably due to the different spatial geometry of QPC used by both groups, asymmetric in Ref. 4 versus symmetric in Ref. 5. Our belief is based on the proposal[6,7] that an asymmetric side-gate voltages ΔV_{SG} can cause the current to become spin polarized due to the spin-orbit interaction (SOI). We expect the same effect can be achieved by a laterally asymmetric geometry for the QPC. Having said that, it is worthwhile to note that such an asymmetric geometry is not a necessary condition for the 0.7 anomaly. The second competing model[8,9] emphasizes the zero-bias peak which it claims to be an evidence of a Kondo-type resonance. This *dynamic* spin flipping is also responsible for the 0.7 anomaly. The preexistence of a moment has been supported by some experiments[10] as well as proved numerically by the spin-density-functional theory.[9] However, this calculation requires the application of a magnetic field beforehand to break the spin symmetry, which step has been subject to criticisms from the rival group.[6]

In contrast to the *lateral* asymmetry due to ΔV_{SG} (Ref. 6) or geometry[4] that creates the spin-polarized current, we wish to show that the source-drain bias (V_{sd}) will break the *longitudinal* symmetry and may lead to the formation of moment in the vicinity of QPC. The ΔV_{SG} may not exist in all experiments that reported the 0.7 anomaly, yet a nonzero V_{sd} is definitely there to determine the conductance. The SOI is needed to argue for the effects of both the lateral and longitudinal asymmetries. But the moment formation further requires a nonuniform electric field in the nonequilibrium Green's-function formalism (NEGF) we employ in this paper. Although the goal of establishing a moment is the same, our approach breaks the spin symmetry by an asymmetric intrinsic SOI instead of an external magnetic field.[9]

II. NEGF FORMALISM FOR QPC

The NEGF is used to calculate the conductance and the density distribution of QPC.[6,11–13] We discretize the space by the lattice constant $a=100$ nm and apply the tight-binding model H_{TB}. The retarded Green's function G^R of the QPC system is given by

$$G_\sigma^R(x,z,E) = (EI - H - \Sigma_S - \Sigma_D - \Sigma_I^\sigma)^{-1}, \tag{1}$$

where G_σ^R is a $2N_xN_z \times 2N_xN_z$ matrix where the N_x and N_z represent the site numbers along x and z directions. The factor of 2 comes from the spin degree of freedom and I is the unit matrix. We assume the leads are normal metal and their interaction with the QPC conducting channel gives rise to the self-energy, Σ_S/Σ_D.[13] The Σ_I^σ denotes the self-energy of spin-σ electron due to the electron-electron interactions. At the lowest order; namely, from the Hartree-Fock terms,

$$\Sigma_I^\sigma(x,z) = \gamma n^{\bar{\sigma}}(x,z) \tag{2}$$

if the screened potential is further approximated by an on-site[11] interaction with strength γ. The $n^{\bar{\sigma}}(x,z)$ denotes the spin density of the opposite spin at the same position. This shows that the Coulomb interaction γ favors spin polarization.

The Hamiltonian $H=H_{TB}+H_{\mathrm{SO}}^\sigma$ in Eq. (1) is composed of the tight-binding H_{TB} and the SOI H_{SO}^σ.[6] Both contribute to

the off-diagonal components, but at different elements because H_{TB} conserves spin while H_{SO}^{σ} flips it. The $H_{TB}(i,j)$ contains the nearest-neighbor hopping energy $t=-\hbar^2/2m^*a^2$ where m^* denotes the effective mass of electrons while the diagonal elements $H(i,i)$ contain the on-site energy $-4t$, electric potential energy $eV(\vec{r}_i)$, and the Zeeman energy. The SOI Hamiltonian $H_{\mathrm{SO}}^{\sigma}=\alpha\vec{\sigma}\cdot\vec{E}\times\vec{k}\equiv\vec{\sigma}\cdot\vec{B}_{\mathrm{SO}}$, where α denotes the spin-orbit interaction strength, $\vec{\sigma}$ the Pauli matrices, $\vec{E}=-\nabla V$ the electric field, and $\vec{k}$ the wave vector. The potential associated with the geometry of QPC is likely to form a bound state in the vicinity of side gates where the electric field is the largest.[14,15]

Initially, we set the γ in Eq. (2) to be zero, i.e., neglecting the Σ_I to obtain a rough estimate of G_{σ}^{R} by Eq. (1). Equipped with this G_{σ}^{R}, we can then follow the standard procedures[6,11] to calculate the lesser Green's function $G_{\sigma}^{<}(x,z,E)$ and spin-density matrix $n^{\sigma}(x,z)$, of different spin σ,

$$G_{\sigma}^{<}(x,z,E)=G_{\sigma}^{R}(x,z,E)\cdot\Sigma^{<}\cdot G_{\sigma}^{A}(x,z,E), \tag{3}$$

$$n^{\sigma}(x,z)=\frac{1}{2\pi}\int G_{\sigma}^{<}(x,z,E)dE, \tag{4}$$

where the advanced Green's function G^A is the Hermitian conjugate of G^R. The lesser self-energy $\Sigma^{<}=f_S\Gamma_S+f_D\Gamma_D$ depends on the Fermi-Dirac function $f_{S/D}(\mu_{S/D})$ and the broadening matrix $\Gamma_{S/D}=-2\,\mathrm{Im}(\Sigma_{S/D})$, which is related to the inverse of the electron lifetime. At the end of this round, we are left with an estimate of $n^{\sigma}(x,z)$ from Eq. (4). Now we turn on the realistic value for γ (to be elaborated in the next section) and repeat the above procedures until $n^{\sigma}(x,z)$ converges. This allows us to finally obtain a self-consistent spin-density matrix, with which we can determine the current I^{σ},

$$I^{\sigma}=\frac{e}{h}\int T(E)[f_S-f_D]dE, \tag{5}$$

where the transmission coefficient $T=\mathrm{Tr}(\Gamma_S G^R\Gamma_D G^A)$.

III. MAGNITUDE OF PARAMETERS

The effective mass of electrons in GaAs is found to be $m^*=0.067m_0$, where m_0 denotes the free electron mass. We set the system size to be $(N_x,N_z)=(19a,13a)$ and all energies in unit of $-t=\hbar^2/2m^*a^2\sim 5.2$ meV. In accordance, the thermal energy at the experimental temperature 1 K will be $k_BT\equiv 1/\beta\sim 1/60$, the electron-electron interaction $\gamma=2\pi a^2$,[6,11] the bottom of conduction band (E_{BC}) at -10, the source-drain bias $eV_{sd}=\mu_S-\mu_D=0.026$ meV~ 0.005, and the Zeeman energy $g_s\mu_B B_{\parallel}\sim 0.01B_{\parallel}$. The size of the SOI constant $\alpha=10^{-3}$ can be determined when we divide the experimentally measured H_{SO} value for GaAs/AlGaAs heterostructures[16,17] by the electric field derived from the potential[15,18] $V(x,z)$ appropriate for QPC.

The potential energy $eV(x,z)$, plotted in Fig. 1, is formed by the voltage V_s on the two charged wires with length $2L=5a$ and separated by a width $W=6a$,

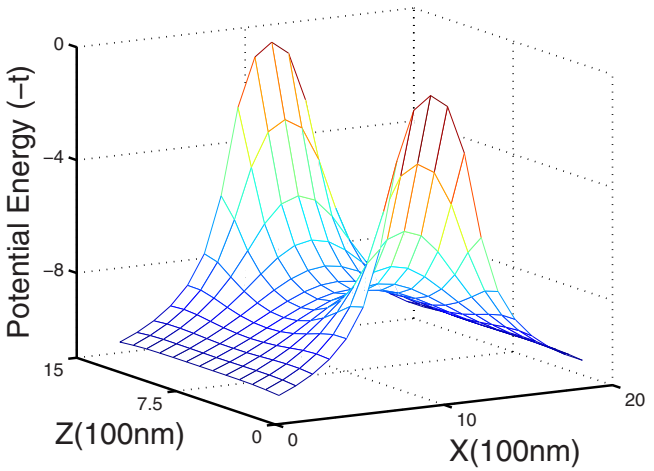

FIG. 1. (Color online) Spatial distribution of potential energy $eV(x,z)+E_{BC}$ due to the side-gate voltage is plotted with $V_{sd}=0.005$ and $V_s=3.1$. The x axis represents the transport direction while z is in its transverse. The contacts of the source/drain leads are at $x=0/19$ columns while the side gates center at $(x,z)=(10,0)$ and $(10,15)$. As can be seen from the figure, the region most influenced by the QPC centers around between $x=6$ and $x=14$.

$$V(x,z)=V_{sd}\frac{L_{sd}-x}{L_{sd}}+V_s\left\{\ln\left[\frac{L-x+\sqrt{(L-x)^2+(z+W)^2+h^2}}{-L-x+\sqrt{(L+x)^2+(z+W)^2+h^2}}\right]+\ln\left[\frac{L-x+\sqrt{(L-x)^2+(W-z)^2+h^2}}{-L-x+\sqrt{(L+x)^2+(W-z)^2+h^2}}\right]\right\}, \tag{6}$$

where L_{sd} denotes the distance between source and drain, $h=0.8a$ is the height of side gates away from the 2DEG. The longitudinal transport direction is along the x axis while the side gates lies in the z direction and forms a conducting channel. We are able to calculate the electric field $\vec{E}$ of H_{SO}^{σ} from $V(x,z,h)$. Side gates forms a symmetric potential along the lateral and longitudinal directions while the potential energy is tilted by the source-drain bias V_{sd}, which breaks the longitudinal symmetry. Combining the asymmetric $V(x,z)$ and the nonuniform SOI will lead to moment formation at the center of the QPC where SOI is the largest. Technically, it is important to include the first term on the right-hand side of Eq. (6) to explicitly break the longitudinal symmetry in order to generate a symmetric spin polarization. This is similar to the effect of ΔV_{SG} at causing the spin-polarized conductance, $0.5G_0$.[6] Otherwise, mere shifting of the chemical potentials on both leads, $\mu_{S/D}=\mu\pm eV_{sd}/2$, still leads to an antisymmetric spin polarization and no net moment is formed around QPC since the hopping amplitude is equal toward all directions. More discussions can be found in the caption of Fig. 6.

IV. NUMERICAL RESULTS

Figure 2 shows the density distribution of spin-up electrons, $n_{\uparrow}(x,z)$, ejected from the source and drain sides. While

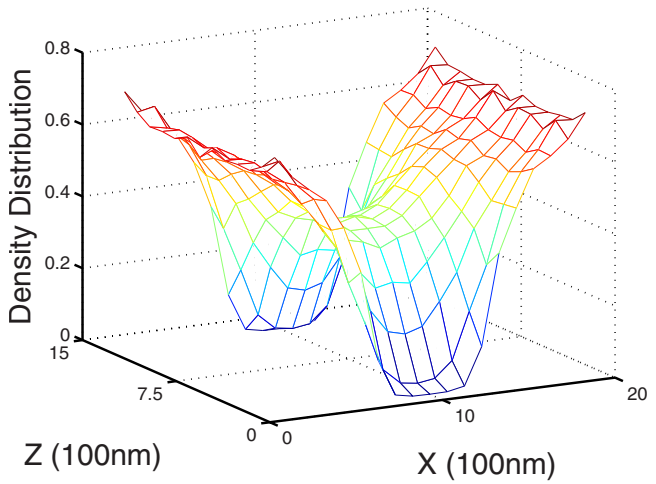

FIG. 2. (Color online) Density distribution of up-spin electrons for $\mu=-3$, $\beta=60$, $V_{sd}=0.005$, $\gamma=2\pi$, and $\alpha=10^{-3}$, injected from the source at $x=1$ and drain at $x=N_x$, under the electric potential energy in Fig. 1.

the density drops upon leaving the leads due to the potential profile in Fig. 1, a conducting channel is formed between the side gates. As we further decrease the Fermi energy μ, this channel will become narrower and eventually get pinched off.

We fix the electric potential while varying μ in Fig. 3, which shows the conductance calculated from Eq. (5). Since the numerical calculations for the self-consistent procedure are very time consuming, we trade the accuracy of the conductance for speed by concluding the program once the resulting conductance gets within the error bar of $0.02/0.2G_0$ for $G=0/1G_0$, respectively. The temperature dependence of the conductance enters via the f_S-f_D term in Eq. (5), which renders the plateau steeper as the temperature is lowered. This tendency is consistent with the experiments.[8] In the mean time, further application of a magnetic field $B_Z=9$ T will lift the spin degeneracy and split the conductance line into two curves due to the Zeeman energy.

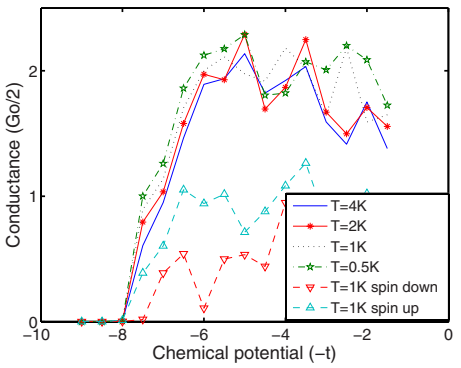

FIG. 3. (Color online) The μ and temperature dependence of the conductance for the QPC described in Fig. 2. The temperature increases from top to bottom, with each line representing temperature $T=4$, 4, 1, and 0.5 K. The tendency to obtain a smoother plateau at high temperature is consistent with experiments. The lowest two curves represent the conductance of spin-up and spin-down electrons in the presence of a magnetic field $B_z=9$ T and at $T=1$ K.

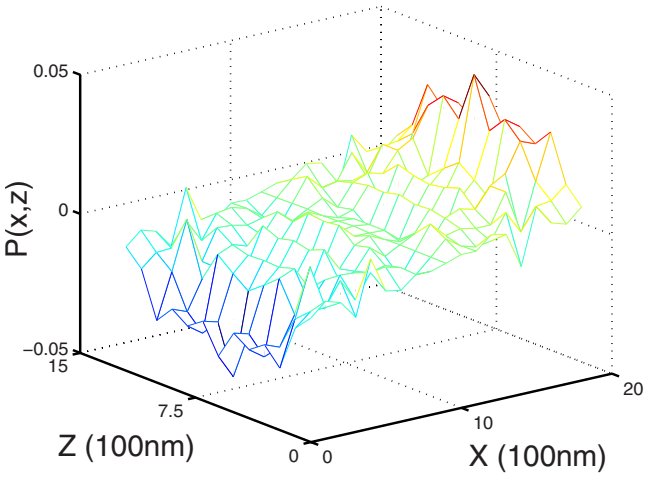

FIG. 4. (Color online) The distribution of spin polarization is plotted for the QPC described in Fig. 2. It is larger at the source and drain because of the Stoner enhancement. Note that the polarization is antisymmetric because its $\mu=-3$ falls below the lowest lateral bound state within the QPC.

The distribution of spin polarization $P(x,z)=(n_\uparrow-n_\downarrow)/(n_\uparrow+n_\downarrow)$ is shown in Fig. 4. According to the Stoner criterion,[19] the polarization is proportional to $\gamma(n_\uparrow+n_\downarrow)^{1/3}$ and, thus, is enhanced at the source and drain where the electron density is higher. For the same reason, a decreasing μ will diminish the spin polarization.

In order to better visualize the moment formation in the vicinity of QPC, we highlight the spin polarization in Fig. 5 in the longitudinal direction at the central row, $z=7$, between the side gates. The chemical potential is now raised above the lowest lateral bound state, which causes the solid line to change from being antisymmetric in Fig. 4 to symmetric. The reason is that the electrons at the center of QPC can now

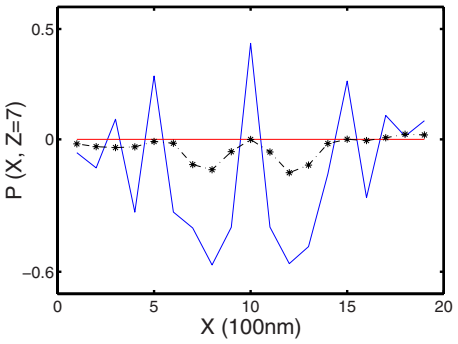

FIG. 5. (Color online) Under the same temperature $\beta=60$ as Fig. 4 but with a higher $\mu=-1.5$, the polarization distribution is plotted along the longitudinal direction at the central row, $z=7$ between the side gates. Except for μ, the solid line shares identical parameters as in Fig. 4. Note that the raise of μ above the lowest lateral bound state within the QPC changes the distribution from being antisymmetric to symmetric. The dashed and asterisk lines correspond to $(\alpha,\gamma)=(0,2\pi)$ and (0.001,0), respectively. The null value of the dashed line signalizes that the SOI is crucial for the moment formation while the asterisk line without γ exhibiting a net polarization between $x=6$ to $x=14$ indicates that the electron-electron interaction is helpful, yet not essential.

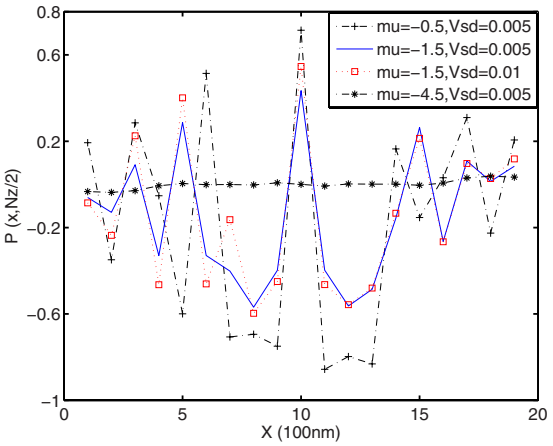

FIG. 6. (Color online) The dependence of spin polarization on μ and $V_{\rm sd}$ at β=60. The solid line, identical to the same solid line in Fig. 5 for $(\mu, V_{sd})=(-1.5, 0.005)$, acts as a reference to the other lines. For the square line, we increase V_{sd}. This leads to a larger conductance and thus a stronger SOI, which enhances the tendency to form a moment. For the cross/asterisk lines, the μ is raised/lowered, which results in an increase/decrease on the polarization.

have a net current flow, which renders the effective magnetic field due to SOI on either side of the QPC to become parallel. Consequently, a net spin polarization or moment formation is favored. To further pin down the driving mechanism behind this phenomenon, we take turns at shutting down the SOI/electron-electron interaction in the dashed/asterisk line. The fact that the dashed line is flat at zero value tells us that the SOI is essential. In contrast, the nonzero polarization of the asterisk line indicates that the electron-electron interaction is dispensable. However, the contrast between the solid and asterisk lines shows that the γ is capable of enhancing the net polarization. This is consistent with our previous conclusion[15] based on the single-particle picture. The oscillatory and decaying behavior away from the center of QPC carries the features of Ruderman-Kittel-Kasuya-Yoshida interaction.[9]

Finally, the μ and V_{sd} dependence of the moment formation is shown in Fig. 6. We use the same solid line in Fig. 5 as a reference. The square line exhibits a higher V_{sd}, which increases the trend for electrons to flow from source to drain and thus leads to more longitudinal asymmetry in $V(x,z)$. The effective magnetic field due to SOI subsequently points in the same direction and breaks the spin degeneracy to induce the polarization. Furthermore, a spatially varying SOI will lead to a nonuniform spin polarization. For QPC, the largest polarization occurs near the center where the SOI is the strongest. The dependence of polarization on μ is tested in the cross and asterisk lines. The former, assigned a higher μ, results in a larger polarization. In contrast, μ in the asterisk line is lowered so much that the electrons on the left/right hop mainly toward the source/drain side. This opposite movement causes the effective magnetic field in either side to point in also opposite directions, which leads to an antisymmetric spin polarization, as is shown by Fig. 4 and the asterisk line. The above conclusions are summarized schematically in Fig. 7.

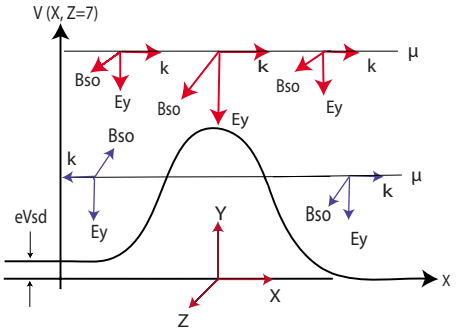

FIG. 7. (Color online) The strength and direction of $\vec{B}_{\rm SO}$ in the QPC are indicated. The thick solid arrows are for μ higher than the potential barrier. This allows the electrons to flow unidirectionally toward the drain, which renders $\vec{B}_{\rm SO}$ pointing at the same direction and a symmetric spin polarization in the longitudinal direction. In addition, the $B_{\rm SO}$ reaches maximum in the vicinity of QPC where the electric field is the strongest. This is also the place where a net moment is expected to be induced, see Fig. 6. In contrast, the thin solid arrows point in opposite directions when μ falls below the lowest lateral bound state. The spin polarization becomes antisymmetry and does not favor forming a net moment, as in Figs. 4 and 6.

V. DISCUSSIONS AND CONCLUSIONS

Compared with our previous approach,[15] several improvements have been made. First, we include the more realistic saddle-point potential to model the confinement through the side gates. Second, we generalize the semiclassical single-particle approach to a full quantum-mechanical one with many-body interactions explicitly accounted for. Third, we emphasize on the dependence of polarization on the source-drain bias and the strength of both the Rashba and electron-electron interactions in this work. This is in contrast to what we did last time; namely, varying the length of QPC and the gate voltage to obtain different degrees of nonuniformity, which led to a switch from the Kondo physics to the Coulomb-blockade one.

In conclusion, we numerically demonstrate that the asymmetric nonuniform SOI in the longitudinal direction is sufficient at inducing a moment in the vicinity of QPC, which is essential in the Kondo-type model for the 0.7 anomaly. Unlike the previous numerical works[9] which relies on a nonzero magnetic field in the beginning to break the spin symmetry, our proposal of an intrinsic SOI is less controversial. The asymmetric SOI is due to the source-drain bias while the nonuniformity comes intrinsically from the side-gate potential. The magnitude of moment depends on the strength of the SOI, electron-electron interaction, the chemical potential, and the source-drain bias. Note that our asymmetry lies in the longitudinal direction, which is in contrast to the lateral one that gives rise to the spin-polarized current.[6]

ACKNOWLEDGMENTS

We thank J. C. Chen, Vidar Gudmundsson, and M. H. Liu for useful discussions, and Shiang Fang for assisting with the Matlab code. Support by the National Science Council in Taiwan under Grant No. 98-2112-M007-005-MY3 is also acknowledged.

[1] B. J. van Wees, H. van Houten, C. W. J. Beenakker, J. G. Williamson, L. P. Kouwenhoven, D. van der Marel, and C. T. Foxon, Phys. Rev. Lett. **60**, 848 (1988).
[2] A very recent survey and discussions on this topic can be found in J. Phys.: Condens. Matter **20**, No. 16 (2008).
[3] K. J. Thomas, J. T. Nicholls, M. Y. Simmons, M. Pepper, D. R. Mace, and D. A. Ritchie, Phys. Rev. Lett. **77**, 135 (1996); D. J. Reilly, T. M. Buehler, J. L. O'Brien, A. R. Hamilton, A. S. Dzurak, R. G. Clark, B. E. Kane, L. N. Pfeiffer, and K. W. West, *ibid.* **89**, 246801 (2002).
[4] L. P. Rokhinson, L. N. Pfeiffer, and K. W. West, Phys. Rev. Lett. **96**, 156602 (2006).
[5] S. M. Frolov, A. Venkatesan, W. Yu, J. A. Folk, and W. Wegscheider, Phys. Rev. Lett. **102**, 116802 (2009).
[6] J. Wan, M. Cahay, P. Debray, and R. Newrock, Phys. Rev. B **80**, 155440 (2009).
[7] P. Debray, S. M. S. Rahman, J. Wan, R. S. Newrock, M. Cahay, A. T. Ngo, S. E. Ulloa, S. T. Herbert, M. Muhammad, and M. Johnson, Nat. Nanotechnol. **4**, 759 (2009).
[8] S. M. Cronenwett, H. J. Lynch, D. Goldhaber-Gordon, L. P. Kouwenhoven, C. M. Marcus, K. Hirose, N. S. Wingreen, and V. Umansky, Phys. Rev. Lett. **88**, 226805 (2002).
[9] Y. Meir, K. Hirose, and N. S. Wingreen, Phys. Rev. Lett. **89**, 196802 (2002); K. Hirose, Y. Meir, and N. S. Wingreen, *ibid.* **90**, 026804 (2003).
[10] Y. Yoon, M.-G. Kang, P. Ivanushkin, L. Mourokh, T. Morimoto, N. Aoki, J. L. Reno, Y. Ochiai, and J. P. Bird, Appl. Phys. Lett. **94**, 213103 (2009).
[11] A. Lassl, P. Schlagheck, and K. Richter, Phys. Rev. B **75**, 045346 (2007).
[12] M. Brandbyge, J.-L. Mozos, P. Ordejon, J. Taylor, and K. Stokbro, Phys. Rev. B **65**, 165401 (2002).
[13] Supriyo Datta, *Electronic Transport in Mesoscopic System* (Cambridge University Press, Cambridge, 1995).
[14] D. Sánchez and L. Serra, Phys. Rev. B **74**, 153313 (2006).
[15] J. H. Hsiao, K. M. Liu, S. Y. Hsu, and T. M. Hong, Phys. Rev. B **79**, 033304 (2009).
[16] Ehud Shafir, Min Shen, and Semion Saikin, Phys. Rev. B **70**, 241302(R) (2004).
[17] J. B. Miller, D. M. Zumbühl, C. M. Marcus, Y. B. Lyanda-Geller, D. Goldhaber-Gordon, K. Campman, and A. C. Gossard, Phys. Rev. Lett. **90**, 076807 (2003).
[18] P. Jaksch, I. Yakimenko, and K.-F. Berggren, Phys. Rev. B **74**, 235320 (2006).
[19] Henrik Bruus and Karsten Flensberg, *Many-Body Quantum Theory in Condensed Matter Physics* (Oxford University Press, New York, 2004).